Proceedings of the ASME 2010 Fluids Engineering Summer Meeting
FEDSM2010
August 1-5, 2010, Montreal, Quebec, Canada

FEDSM-ICNMM2010-31192

NUMERICAL MODELING OF MINI/MICROCHANNEL REACTOR FOR METHANE-STEAM REFORMING

Daniel Peterson
School of Mechanical, Industrial and Manufacturing Engineering
Oregon State University
Corvallis, Oregon 97331
Email: dpeterso@engr.orst.edu

Sourabh V. Apte
School of Mechanical, Industrial and Manufacturing Engineering
Oregon State University
Corvallis, Oregon 97331
Email: sva@engr.orst.edu

Vinod Narayanan
School of Mechanical, Industrial and Manufacturing Engineering
Oregon State University
Corvallis, Oregon 97331
Email: vinod.narayanan@oregonstate.edu

John Schmitt
School of Mechanical, Industrial and Manufacturing Engineering
Oregon State University
Corvallis, Oregon 97331
Email: schmitjo@engr.orst.edu

ABSTRACT

Numerical modeling of methane-steam reforming is performed in a mini/microchannel with heat input through Nickel-deposited channel walls. The low-Mach number, variable density Navier-Stokes equations together with multicomponent reactions are solved using a parallel numerical framework. Methane-steam reforming is modeled by three reduced-order reactions occurring on the reactor walls. The surface reactions in the presence of Nickel catalyst are modeled as Neumann boundary conditions to the governing equations. Effects of the total heat input, heat flux profile, and inlet methane-steam molar concentration on production of hydrogen are investigated in detail.

NOMENCLATURE

A Pre-exponential constant, $[kmol/m^2-s]$
A_c Cross sectional area of the physical plant, $[m^2]$
C_i Concentration of the i^{th} chemical species, $[kmol_i/m^3]$
c_p Specific heat, $[kJ/kg-K]$
$\mathscr{D}_{i,m}$ Binary diffusion coefficient, i corespondents to the chemical species, $[m^2/s]$
$E_{a,k}$ Activation energy of the k^{th} reaction, $[kJ/mol]$
h Specific enthalpy of mixture, $[kJ/kg]$
$h^o_{f_i}$ Specific enthalpy of formation of the i^{th} species, $[kJ/kg]$
ΔH^0_{298} Specific heat of reaction at reference temperature $298K$, $[kJ/mol]$
$\Delta H_{R,k}$ Specific heat of reaction of the k^{th} reaction, $[kJ/mol]$
k Thermal conductivity of mixture, $[kW/m-K]$
k_f Specific reaction rate constant,$[kmol/m^2-s]$
$\mathscr{M}_i$ Molecular weight of species i, $[kg_i/kmol_i]$
$\mathrm{N_s}$ Number of chemical species
n Wall normal direction
p Pressure, $[Pa]$
q_j Heat flux due to conduction and species diffusion, $[kW/m^3]$
$\dot{Q}_{total}$ Flow rate of both inlet methane and steam, $[ml/min]$
r_k Reaction rate of k^{th} reaction, $[kmol/m^2-s]$
$\dot{s}_i$ Rate of chemical species adsorption and desorption at the catalyst surface of species i, $[kmol_i/m^2-s]$
R Universal gas constant, $[kJ/kmol-K]$
t Time, $[s]$

T Absolute temperature, $[K]$
u_i Velocity in tensor notation where $i = 1,2,3$ corespondents to the x, y and z directions, $[m/s]$
$\overline{u}$ Mean velocity in the x direction, $[m/s]$
x_i Direction of the i^{th} directions, $[m]$
Y_i Species mass fraction of species i, $[kg_i/kg_{mixture}]$
$Y_{bulk,i}$ Bulk species mass fraction of species i, $[kg_i/kg_{mixture}]$
α Temperature exponent, [1]
μ Viscosity of mixture, $[kg/m-s]$
ν''_{ki} Stoichiometric coefficient of the i^{th} chemical species in reaction k of reactants, [1]
ν'_{ki} Stoichiometric coefficient of the i^{th} chemical species in reaction k of products, [1]
Φ_v Viscous dissipation, $[N/m^2-s]$
ρ Density of mixture, $[kg/m^3]$
$\dot{\omega}'''_i$ Reaction rate of the k^{th} reaction, $[mol_i/m^2-s]$

INTRODUCTION

The present work investigates conversion efficiency of biomass-based gaseous products (CH_4,CO_2) using a micro/mini-channel reactor. This design exploits the short diffusion lengths for reactant gases in microchannels, such that the reaction may occur near stoichiometric conditions (using very less excess reactant gases), thereby substantially increasing the efficiency of the system. Such a design has several advantages: (a) reduced mixing time for non-premixed reactants since diffusion time is limited by the cross-section of microchannels, (b) very high heat transfer rates in microchannels, and (c) damage to one of the microchannels does not cause catastrophic failure of the reactor.

In order to study the technical feasibility of such a design, we first investigate, through numerical simulations, the strong endothermic reactions of methane-steam reforming inside a micro/mini-channel reactor with *Nickel* catalyst. The low-Mach number, unsteady, variable-density Navier-Stokes equations together with species mass-fraction and energy equations are solved in a microchannel. The surface chemical reactions are modeled as boundary conditions to the energy and species equations for a reduced reaction mechanism of methane-steam reforming [1, 2, 2–4]:

$$\mathrm{CH_4 + 2H_2O \Longleftrightarrow CO_2 + 4H_2;} \quad \Delta \mathrm{H^0_{298} = +165\ kJ/mol} \quad (1)$$
$$\mathrm{CO + H_2O \Longleftrightarrow CO_2 + H_2;} \quad \Delta \mathrm{H^0_{298} = -41\ kJ/mol} \quad (2)$$
$$\mathrm{CH_4 + H_2O \Longleftrightarrow CO + 3H_2;} \quad \Delta \mathrm{H^0_{298} = +206\ kJ/mol.} \quad (3)$$

There have been several studies on micro/minichannels reactors with Rhodium, Palladium or Nickel catalysts arranged in the form of a packed bed [3–6]. Recently, Wang *et. al.* [2] investigated the effects of steam-methane inlet ratio and flow rates on hydrogen production, in a planar solid-oxide fuel cells (SOFC) using experimental and numerical modeling in steady-state. Kuznetsov & Kozlov [1] investigated the effect of heat flux distribution on methane-steam reforming using reduced reaction mechanisms in a microchannel with Nickel catalyst. The goal of this work is to investigate the effect of inlet steam-methane ratio, the distribution and amount of external heat flux on the physicochemical reactions, species diffusion, and heat transfer processes inside the microchannel reactor. Accordingly, the parameters varied in this work are the heat flux magnitude ($|\dot{q}''|$), heat flux profile ($\dot{q}'' = f(x)$), steam-methane ratio ($S:M$) and total flow rate ($\dot{Q}$). The microchannel geometry is chosen based on the work by Wang *et. al.* [2] and their experimental data is used to first validate the numerical model.

Mathematical Formulation

The mathematical formulation is based on the variable-density, Navier-Stokes equations together with species mass-fraction and enthalpy equations [7]:

$$\frac{\partial \rho}{\partial t} + \frac{\partial}{\partial x_j}(\rho u_j) = 0; \quad (4)$$
$$\frac{\partial \rho u_i}{\partial t} + \frac{\partial}{\partial x_j}(\rho u_i u_j) = -\frac{\partial p}{\partial x_i} + \frac{\partial \tau_{ij}}{\partial x_j}; \quad (5)$$
$$\frac{\partial \rho Y_i}{\partial t} + \frac{\partial}{\partial x_j}(\rho u_j Y_i) = \frac{\partial}{\partial x_j}\left(\rho \mathscr{D}_{i,m} \frac{\partial Y_i}{\partial x_j}\right) + \dot{\omega}'''_i;\ \mathrm{i = 1...N_s} \quad (6)$$
$$\frac{\partial \rho h}{\partial t} + \frac{\partial}{\partial x_j}(\rho u_j h) = -\frac{\partial q_j}{\partial x_j} + \mu \Phi_v; \quad (7)$$

where N_s, ρ, u_i, Y_i, p, h, q_j, and Φ_v represent the number of species transport equations, density, velocity components, species mass fraction, pressure, total enthalpy, heat flux due to conduction and species diffusion, and viscous dissipation, respectively. The mixture is assumed as an ideal gas with the viscosity, thermal conductivity, and the binary diffusion coefficient ($\mathscr{D}_{i,m}$) depending upon the local composition and temperature. The mixture density is obtained from the equation of state for an ideal gas,

$$p = \frac{\rho RT}{\mathscr{M}_{mixture}}, \quad (8)$$

where, R is the universal gas constant, p is the operating pressure, and T is the mixture temperature. The mixture molecular weight is given by the expression, $\mathscr{M}_{mixture} = (\sum_i^{N_s} \frac{Y_i}{\mathscr{M}_i})^{-1}$, where N_s is the total number of species.

The gas-phase reaction rates ($\dot{\omega}'''_i$) are functions of temperature, species concentration, and pressure field [5, 6]. The total

enthalpy h is given as

$$h = h^o_{f_{mix}} + \int_{T_{ref}}^{T} c_{p_{mix}} dT; \quad h^o_{f_{mix}} = \sum_{i}^{N_s} Y_i h^o_{f_i}. \tag{9}$$

Where, h is the total enthalpy of the mixture, $h^o_{f_{mix}}$ is the enthalpy of formation of the mixture, $h^o_{f_i}$ is the enthalpy of formation for the i^{th} species, $c_{p_{mix}}$ is the specific heat of the mixture (the mass weighted average of the species' specific heat), N_s is the total number of species and T_{ref} is a reference temperature.

Chemical Kinetics and Surface Reactions

In the microchannel-based solar reactor, chemical reactions can occur in the gaseous phase as well as a series of reactions on the catalyst surface. Past studies by Deutschmann & Schmidt [5] on oxidation of steam in a tubular model showed that for atmospheric pressures, the gas-phase reactions contributed negligibly to the oxidation process; however, increase in reactor pressure beyond 10 bar resulted in sensitivity of the oxidation process to the gas-phase reactions. In the present work, we perform numerical experiments at atmospheric conditions and neglect the gas-phase reactions. The numerical solver presented in this work is, however, capable of accounting for the gaseous-phase chemical kinetics.

The catalytic reaction rates are nonlinear relations comprising the reactant species concentrations and the local temperature. Modeling of detailed chemical kinetics pathways for catalytic reactions on the surface have been performed [5, 8]; however, can become prohibitively expensive for time-resolved simulations performed in the present work. A reduced reaction mechanism with the following two endothermic (equations 3,1) and one exothermic water-gas shift (equation 2) global reactions was used to model the chemical conversion.

To calculate the reaction rates, the classical kinetic model was employed, wherein the reaction rates for each chemical reactions can be formulated as [9, 10],

$$r_k = k_{f,k} \Pi_{i=1}^{N_s} [\mathrm{C}_i]^{\nu'_{ki}}, \tag{10}$$

$$k_{f,k} = A_k \exp\left(-\frac{E_{a,k}}{RT}\right), \tag{11}$$

where C_i denotes the concentration per unit volume of the i^{th} chemical species in the mixture, $k_{f,k}$ is the specific reaction rate constant for the k^{th} reaction and ν'_{ki}, which is dimensionless, is the stoichiometric coefficient of the i^{th} chemical species in the k^{th} reaction. Experimental data for the reaction activation energy ($E_{a,k}$), the activation constants A_k and α_k for each k^{th} reaction is obtained from the experimental data [3,4]. It should be noted that the predictive capability of the numerical approach depends on accurate characterization of the surface reactions rates. Detailed chemical kinetics pathways for catalytic surface reactions [5, 8] were used in the modeling of the catalytic reaction on the channel surface. In the present work, we use a reduced reaction mechanism to reduce the computational cost. There have been previous studies on methane-steam reforming [2] and Kutnetsov [1] using similar three-step reduced reaction mechanism.

With the above surface reaction rates, the catalytic conversion is then modeled simply through the following boundary conditions for the species mass-fractions and temperature equations [1, 5]:

$$-\rho \mathscr{D}_i \frac{\partial Y_i}{\partial n} = \dot{s}_i \mathscr{M}_i; \quad -k\frac{\partial T}{\partial n} = q_{wall} + \sum_{k}^{3} r_k \Delta H_{R,k}, \tag{12}$$

where $\dot{s}_i$ is the rate of chemical species adsorption and desorption at the catalyst surface, $\mathscr{M}_i$ is the molecular weight of species i, q_{wall} is the rate of external heat supplied to the wall, $\Delta H_{R,k}$ is the heat of reaction, r_k is the reaction rate of the k^{th} surface reaction. The surface adsorption and desorption rates depend on the coverage of the catalyst over the surface and surface site density [1, 5, 6]. In the present work, uniform catalyst surface density is assumed for the reactor conditions. The surface adsorption/desorption rates for each i^{th} species are obtained as:

$$\dot{s}_i = \sum_{k=1}^{3} \left(\nu'_{ki}(r_k) - \nu''_{ki}(r_k)\right), \tag{13}$$

where is the summation is over the three chemical reactions in the reduced reaction mechanism.

Numerical Implementation

For the numerical implementation, it is assumed that the flow velocity is much smaller than the speed of sound and the mean thermodynamic pressure field within the microreactor remains approximately constant, such that the zero-Mach number assumption is valid. The numerical solver is based on a pressure-based, reacting flow solver on unstructured grids [11–14]. The flow solver has been used for two-phase reacting flow field in a realistic gas-turbine combustor and is able to capture the reaction dynamics in the microchannel configuration. The solver is three-dimensional, massively parallel and is suitable for large number of parameter variation studies.

The governing equations are solved using a fractional-step method. First, the scalar fields (the species concentrations and temperature fields) are solved in a conservative form using a third or WENO discretization [11, 14]. The new scalar fields are used to evaluate new mixture density using the ideal gas law. The momentum and continuity equations are solved using a pressure-based, predictor-corrector approach. The momentum equation is

used to first predict a new velocity field. This velocity field is then corrected by solving a pressure-Poisson equation constraining the velocity field to satisfy the continuity constraint. The details of the numerical approach are given in [11,13,14]. In the present work, the total enthalpy equation is re-written in the form of a transport equation for the sensible enthalpy. This leads to a reaction source term based on the heats of formation of species in the gaseous phase. In the present work, gas-phase reactions are neglected. The catalytic surface reactions are modeled through boundary conditions for the gas-phase species.

Numerical Results

Figure 1 shows the schematic of the computational domain with the height and spanwise length of 4.5 mm axial flow length of 0.13 m. A porous nickel catalyst section, on the top and bottom walls starts at flow length of 0.015 m and continues up to 0.115 m. This catalyst configuration allows the flow to develop before the reaction zone. The Reynolds number varies between simulations but is always in the laminar flow regime. A structured Cartesian grid was used in this simulation with 25×800 control volumes in the vertical and axial directions, respectively. For the present study, variations in spanwise directions were assumed negligible, and a two-dimensional configuration is assumed.

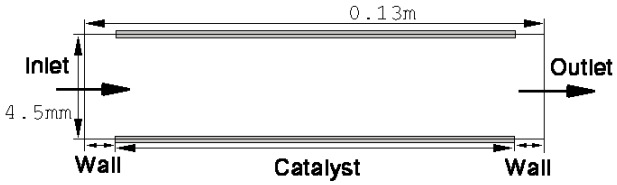

FIGURE 1. Schematic of the mini-channel reractor with catalyst on the top and bottom surfaces. A two-dimensional approximation is used in numerical studies.

In this zero-Mach number variable density reacting flow computation, the reactor pressure is assumed constant at 100 kPa. The inlet temperature is set to 973 K for all cases. The total heat flux ($|\dot{q}''|$), the heat flux profile ($\dot{q}'' = f(x)$), the inlet steam-methane ratio (S:M), and the inlet flow rate ($\dot{Q}$) are varied and their effects on H_2 production are investigated. A uniform inlet velocity field (based on the flow-rate and inlet area) together with Dirichlet conditions for the species mass fractions (based on the steam-methane ratio) are specified. A convective boundary condition is imposed at the outlet section. No-slip conditions are assumed on the walls. For regions with no catalyst a zero-flux Neumann condition is employed for the species mass-fractions and temperature fields. For the catalyst region, the species mass-fractions and temperature conditions are based on the catalytic reactions (equation 12).

Characterization of Porosity of Catalyst Surface

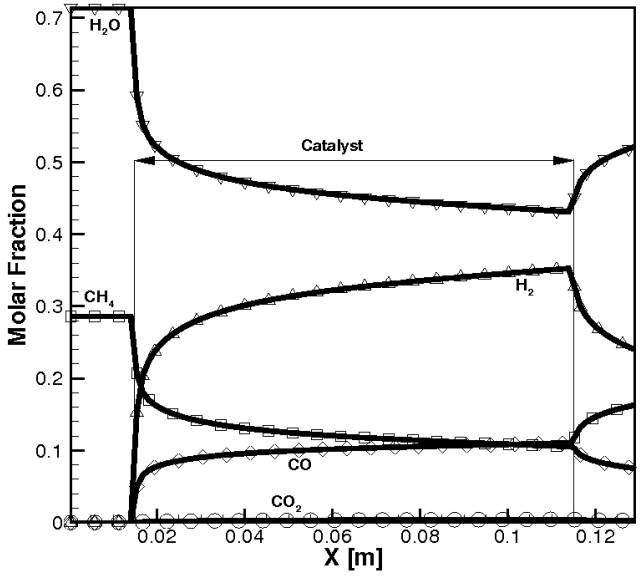

(a) Chemical Species

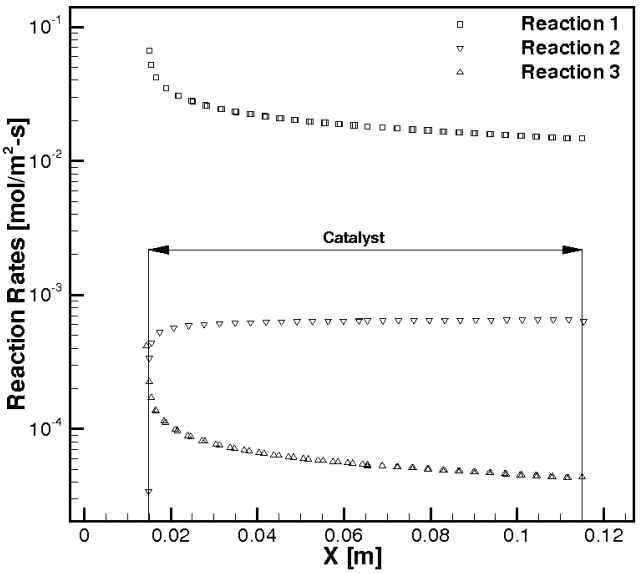

(b) Reaction Rates

FIGURE 2. Variation of species concentrations along the microchannel reactor (a) and reaction rates along the microchannel reactor (b). The flow rate is 800 ml/min, steam-methane ratio is 2.5 and constant wall temperature is 973 K.

TABLE 1. Exit hydrogen concentration and percentage CH_4 consumption for various flow rates compared with experimental data [2].

Flow Rate	X_{H_2} [2]	Present X_{H_2}	% CH_4 consumption [2]	Present % CH_4 consumption
ml/min	Molar Fraction	Molar Fraction	%	
100	0.515	0.503	87.5	89.0
200	0.486	0.444	81.5	78.0
300	0.451	0.412	75.2	73.3
400	0.423	0.400	67.5	69.9

Accurate characterization of the reaction on the catalyst surface is critical to correctly predict the chemical conversion in the microchannel reactor. Given the complexity of the surface reaction mechanisms in the presence of a porous catalyst, it is difficult to completely model the diffusion and chemical reactions through the porous surface. The reaction-rates predicted by the equations 1, 2 and 3 for a non-porous catalyst are first calibrated against the experimental data by Wang *et al.* [2] on microchannel methane-steam reforming for a porous catalyst. These reaction rates are then used to predict the hydrogen production for different cases studied experimentally [2] to show good agreement with the experimental data. Wang *et al.* [2] also used a similar procedure for their numerical simulations. Accordingly, for a flow-rate of 800 ml/min, constant wall temperature of 973 K and inlet steam-methane ratio of 2.5, the reaction rates were calibrated to match the exit bulk molar concentrations of H_2. The bulk mass-fractions at a channel cross-section is defined as,

$$Y_{bulk,H_2} = \frac{1}{A_c \overline{u}} \int_A u Y_{H_2} dA. \tag{14}$$

where $\overline{u}$ is the average velocity at the cross-section. With this input from the experimental data, a series of runs at varied flow-rates were conducted to predict the exit hydrogen concentrations and compared with the experimental data in Table 1 to show reasonable match.

Figure 2a shows the molar fractions of all species along the microchannel wall for the inlet flow-rate of 800 ml/min. For this high flow rate, it is seen that hte conversion of CH_4 to H_2 is not complete over the microchannel length. The molar fraction variations shown are on the catalyst surface. Downstream of the catalyst, the molar fractions of H_2O and CH_4 near the catalyst surface increase. This is mainly because of diffusion of methane and steam from the centerline of the microchannel to the channel walls. However, because of lack of catalyst there are no reactions. Figure 2b shows the distribution of reaction rates for the three chemical reactions considered. It is observed that the first reaction (equation 3) is most dominating compared to the exothermic water gas shift reaction and the other reaction producing CO. Figure 3 shows the dominant reaction rate for different flow rates. For lower flow-rates, and thus with increased convective residence time, the reactions to go to completion and majority of the methane is consumed to produce H_2 as expected.

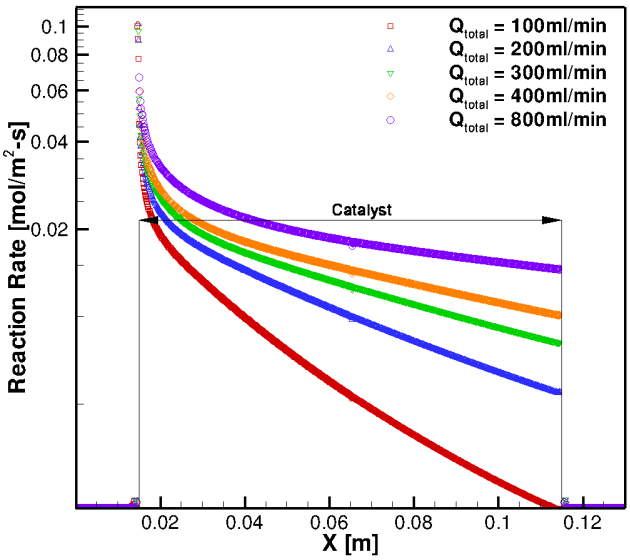

FIGURE 3. Variation of surface reaction rates for different flow-rates and a steam-methane ratio of 2.5 with constant wall temperature of 973 K.

Magnitude Heat Flux

The reaction rates are highly dependent on the local temperature. Here, we investigate the effect of external heat flux on H_2 production. Four heat flux magnitudes were enforced at mean values of 0, 1, 2 and 3 kW/m^2. The heat flux is also linearly increasing along the channel wall. The steam-methane ratio was set to 2.5 and the flow rate for these cases is maintained at $400ml/min$. It is found that, with increase in the amount of heat flux, the H_2 production as well as reaction rates at the wall increase. Increased value of heat flux increases the temperature

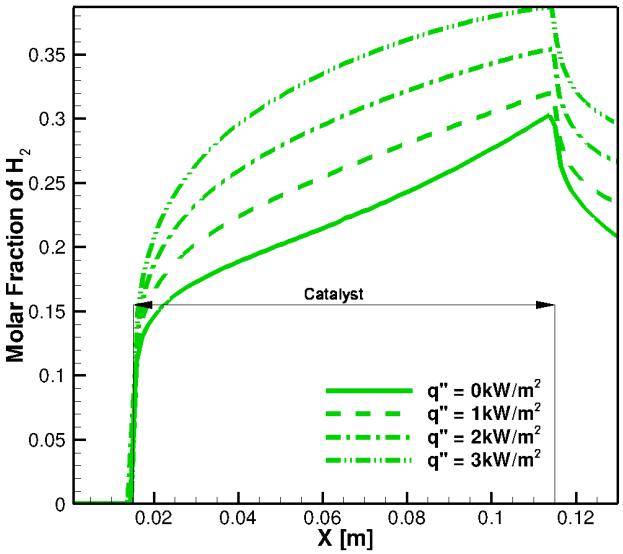

(a) H_2 Concentration

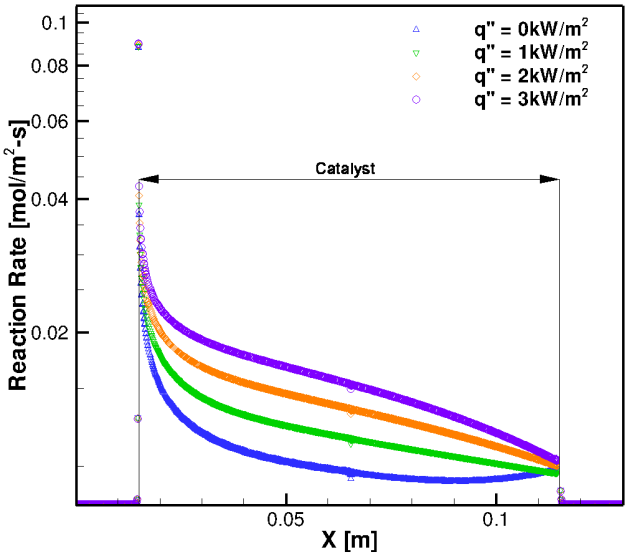

(b) Reaction Rate of Reaction 1

FIGURE 4. Variation of H_2 concentration (a) and reaction rate (b) along the microchannel reactor for different wall heat fluxes.

along the wall, leading to enhanced H_2 production. The reaction rates plot indicates a peak in their values at the beginning of the catalyst surface. The premixed H_2O-CH_4 mixture diffuses to the catalyst surface and reacts to produce hydrogen. Production of H_2 is an endothermic reaction, and this causes the temperature at the wall to initially decrease. Reactions continue to occur along the channel wall, however, their rate is decreased. The amount of methane and steam diffusing to the channel wall are also affected with production of H_2 in the upstream section. Since the inlet temperature of the premixed mixture is relatively high, reactions are initiated even for the case of no heat flux; however, the amount of H_2 produced is considerably lower compared to high heat flux cases. The variation of H_2 molar fraction shows a decrease after the catalyst section. This is mainly because of diffusion of H_2 produced at the wall to the centerline of the channel; however, the bulk H_2 molar fraction remains the same after the catalyst section.

Heat Flux Profile

Since methane-steam reforming is an endothermic reaction, the temperature values near the catalyst wall are bound to drop in the absence of heat addition. However, in order to explore the effect of heat-flux profile on the non-linear nature of the reaction rates and H_2 production, we considered three different heat flux profiles: uniform distribution, ramp up, and ramp down wherein the heat flux is varied linearly along the channel walls. For all cases, the average heat flux over the microchannel length is kept fixed at 2 kW/m^2 and the steam-methane ratio was set to 2.5 at a flow rate of $400 ml/min$. Figures 5 show the variation of H_2 molar concentrations along the channel together with wall temperature for the three different heat flux profiles. It is observed that, for all heat flux profiles, the temperature drops in the upstream section of the channel where the reaction rates are large. The ramp down heating, however, does not raise the temperature of the wall sufficiently to produce higher H_2 concentrations. Small increase in temperature occurs mainly because the endothermic reaction rates are smaller and also there is heat addition. The ramp-up distribution, seems to give increased production of H_2. It should be noted that in the present microchannel, the conversion of CH_4 is not complete for the flow rate of 400 ml/min. This indicates that a longer microchannel is needed for complete conversion.

Steam Methane Ratio

Finally we vary the inlet steam-methane ratio for a flow rate of 400 ml/min and average heat flux of 2 kW/m^2. The heat flux profile is linear ramp-up along the channel wall. The reaction rates are non-linear functions of the reactant concentrations. Owing to the three-step reduced reaction kinetics studied here, we define the optimal steam-methane ratio as the averaged ratio of the stoichiometric coefficients for steam and methane weighted by the corresponding reaction rates for all three reactions. It was found that, a steam-methane ratio of approximately 3.0 (on molar basis) provides the maximum H_2 production as seen from figure 6.

Conclusion

Numerical experiments investigating effectiveness of a mini/microchannel reactor geometry on methane-steam reforming are performed using a low-Mach number, variable den-

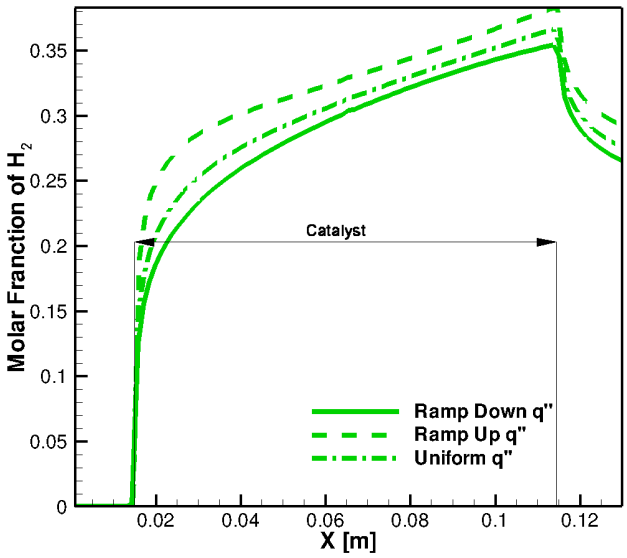

(a) H_2 Concentration

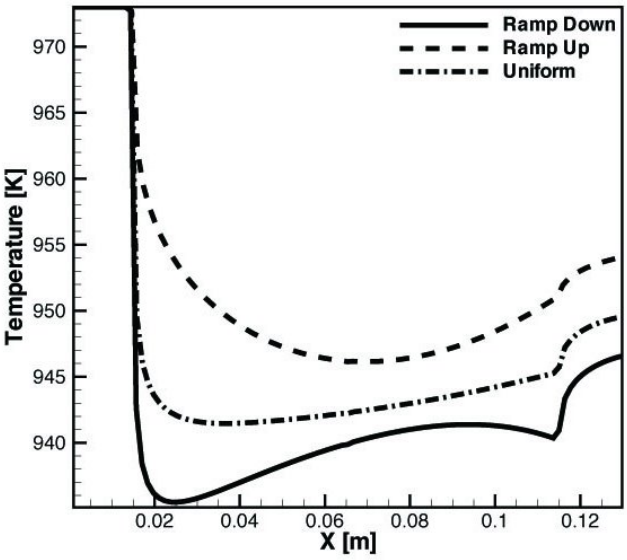

(b) Wall Temperature

FIGURE 5. Variation of H_2 Molar concentration (a) and wall temperature (b) along the channel wall for different heat flux profiles. The average heat flux is kept constant at 2 kW/m^2, the flow rate is 400 ml/min and steam-methane ratio is 2.5.

sity Navier-Stokes equations together with multicomponent reactions. Methane-steam reforming is modeled by three reduced-order reactions occurring on the reactor walls, two of which are endothermic reactions and an exothermic water-gas shift reaction. The reaction rate constants are for a Nickel-deposited catalyst. The reaction rate constants are obtained based on the experimental work by Wang *et al.* [2] and are matched for a high

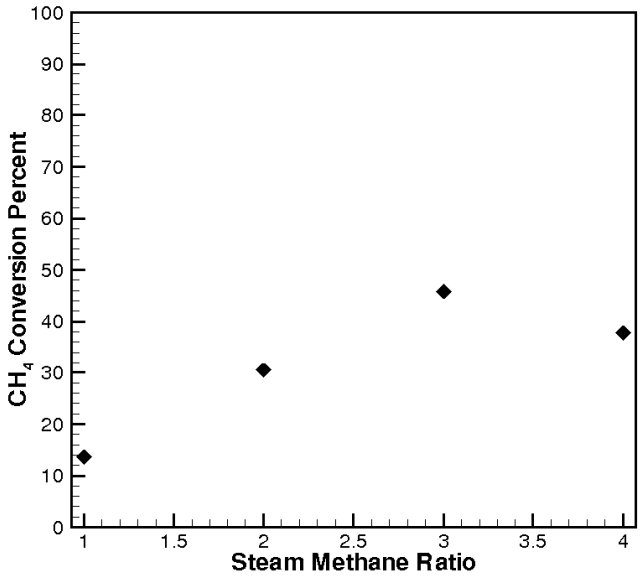

FIGURE 6. Effect of varying the inlet steam-methane ratio on H_2 production at flow rate of 400 ml/min and average heat flux of 2 kW/m^2.

flow-rate constant wall temperature case. The predictions of the numerical simulation are first validated against the experimental data for different flow rates to show reasonable agreement of H_2 production and methane consumption.

The validated numerical model, was then applied to perform parametric studies investigating effect on hydrogen production. The amount of heat flux, the heat flux profile, and the steam-to methane ratio were varied for a fixed total mass-flow rate. It was found that, for all cases majority of the conversion to H_2 takes place in the upstream section of the microchannel where the reaction rates are considerably large. With production of products such as CO and CO_2 and H_2, the reaction rates drop along the length of the channel. It was found that manipulating the wall heat flux profile can result in optimal H_2 production for a specific steam-methane ratio. It was also found that accurate quantification of the reaction rates and porosity of the catalyst surface are critical for numerical model predictions. Ongoing work at OSU involves experimental measurements of catalytic reaction rates in the presence of Palladium catalyst. This data will then be used to investigate response to temporal variations in heat fluxes and heat flux profiles on H_2 production using solar energy.

The above results were obtained in a mini-channel; however, studies are currently being performed in using microchannels minimizing the diffusion time-scales in the reactor.

ACKNOWLEDGMENT

This work was funded in part by the Oregon Best Solar energy initiative and partly by the seed grant from OSU's School of

Mechanical Industrial and Manufacturing Engineering. We also thank Prof. Murty Kanury of OSU for several useful discussions related to combustion and chemical kinetics modeling.

REFERENCES

[1] Kuznetsov, V., and Kozlov, S., 2008. "Modeling of methane steam reforming in a microchannel with a heat flow distributed in length". *Journal of Engineering Thermophysics,* ***17***(1), pp. 53–59.

[2] Wang, Y., Yoshiba, F., Kawase, M., and Watanabe, T., 2009. "Performance and effective kinetic models of methane steam reforming over Ni/YSZ anode of planar SOFC". *International Journal of Hydrogen Energy,* ***34***(9), pp. 3885–3893.

[3] Xu, J., and Froment, G., 1989. "Methane steam reforming, methanation and water-gas shift: I. Intrinsic kinetics". *AIChE Journal,* ***35***(1), pp. 88–103.

[4] Hou, K., and Hughes, R., 2001. "The kinetics of methane steam reforming over a Ni/α-Al2O catalyst". *Chemical Engineering Journal,* ***82***(1-3), pp. 311–328.

[5] Deutschmann, O., and Schmidt, L., 1998. "Modeling the partial oxidation of methane in a short-contact-time reactor". *AIChE Journal,* ***44***(11), pp. 2465–2477.

[6] Appel, C., Mantzaras, J., Schaeren, R., Bombach, R., Inauen, A., Tylli, N., Wolf, M., Griffin, T., Winkler, D., and Carroni, R., 2005. "Partial catalytic oxidation of methane to synthesis gas over rhodium: in situ raman experiments and detailed simulations". *Proceedings of the Combustion Institute,* ***30***(2), pp. 2509 – 2517.

[7] Bird, R., Stewart, W., and Lightfoot, E. "Transport Phenomena, Wiley, New York, 1960".

[8] Stutz, M. J., and Poulikakos, D., 2005. "Effects of microreactor wall heat conduction on the reforming process of methane". *Chemical Engineering Science,* ***60***(24), pp. 6983 – 6997.

[9] Kenneth, K., 2005. "Principles of combustion". *John Wiley's sons, Ine, Hoboken, New Jersey*.

[10] Turns, S., 1995. "An introduction to combustion: Concepts and applications(Book)". *New York: McGraw-Hill, Inc, 1995*.

[11] Moin, P., and Apte, S., 2006. "Large-eddy simulation of realistic gas turbine combustors". *AIAA Journal,* ***44***(4), pp. 698–708.

[12] Apte, S., Mahesh, K., Moin, P., and Oefelein, J., 2003. "Large-eddy simulation of swirling particle-laden flows in a coaxial-jet combustor". *International Journal of Multiphase Flow,* ***29***(8), pp. 1311–1331.

[13] Mahesh, K., Constantinescu, G., Apte, S., Iaccarino, G., Ham, F., and Moin, P., 2006. "Large-eddy simulation of reacting turbulent flows in complex geometries". *Journal of Applied Mechanics,* ***73***, p. 374.

[14] Ham, F., Apte, S., Iaccarino, G., Wu, X., Herrmann, M., Constantinescu, G., Mahesh, K., and Moin, P., 2003. "Unstructured LES of reacting multiphase flows in realistic gas turbine combustors. Annual Research Briefs 2003". *Center for Turbulence Research, NASA Ames/Stanford Univ*, pp. 139–160.